



Article

Flexo-ionic Effect of Ionic Liquid Crystal Elastomers

C. P. Hemantha Rajapaksha ¹, M. D. Tharindupriya Gunathilaka ², Suresh Narute ³, H. A. Albehaijan ³, Camilo Piedrahita ³, P. Paudel ¹, Chenrun Feng ², Björn Lüssem ¹, Thein Kyu ³ and Antal Jákli ^{1,2,*}

- ¹ Department of Physics, Kent State University, Kent, OH 44240, USA
- Advanced Materials and Liquid Crystal Institute, Kent State University, Kent, OH 44240, USA
- ³ Department of Polymer Engineering, University of Akron, OH 44325, USA
- * Correspondence: ajakli@kent.edu

Abstract: The first study of the flexo-ionic effect, i.e., mechanical deformation induced electric signal of the recently discovered ionic liquid crystal elastomers (iLCEs) is reported. The measured flexo-ionic coefficients were found to strongly depend on the director alignment of the iLCE films and can be over 200 μ C/m. This value is orders of magnitude higher than the flexoelectric coefficient found in insulating liquid crystals and is comparable to the well-developed ionic polymers (iEAPs). The shortest response times, i.e., the largest bandwidth of the flexoionic responses is achieved in planar alignment, when the director is uniformly parallel to the substrates. These results render high potential for iLCE-based devices for applications in sensors and wearable micropower generators.

Keywords: ionic liquid crystal elastomers; ionic liquids; flexoelectricity; flexo-ionic effect; micropower generation; sensors; electromechanical coupling

1. Introduction

The past few decades have witnessed a flourishing development in electromechanical transducers for use in soft robotics ^{1–3}, sensors ^{4,5} and micro power generations ^{6–9}. Piezoelectricity and flexoelectricity are the two major physical mechanisms for linear electromechanical transduction for insulating materials. Piezoelectricity is restricted only to non-centrosymmetric materials and linearly couples mechanical strain and electric signals ¹⁰

Flexoelectricity exists even in centrosymmetric materials by coupling electric polarization with strain gradient. It has been studied in both solid crystals and liquid crystals since the 1960s 11 . In crystalline solids, the induced electric polarization is attributed to the displacement of electrons. The highest flexoelectric coefficients in the range of 1- 100 μ C/m have been reported for ferroelectric ceramics 12,13 , whereas in dielectric polymers the values are several order of magnitudes smaller, in the range of 10^{-2} - 10^{-3} μ C/m 14,15 . In liquid crystals the dipolar origin of the flexoelectricity arises when the director structure of dipolar pear (tear drop) or bent (banana) shape molecules suffer splay or bend distortions, respectively 11 . The flexoelectric coupling coefficients arise from such dipolar contribution were measured to be very low, i.e., 1-10 pC/m 16,17 . Later a three orders of magnitude larger effect (\sim 60 nC/m) was observed in bent-core liquid crystals, but that was attributed to strain gradient induced reorientation of 10-100 nm scale ferroelectric smectic clusters 18 . Bent core nematic liquid crystal elastomers have also been shown to show a large (\sim 30 nC/m) flexoelectric coefficient 19 . They are much less brittle than rigid ceramics and are self-standing and rugged unlike fluid nematics.

In past two decades, ionic electroactive polymers (iEAPs), have drawn widespread attention due to their unique properties that can be used in soft robotics as actuators^{20–24} and sensors^{24,25}. In these systems, due to the different sizes of the anions and cations, the applied voltage leads to a mechanical bending and, conversely, a mechanical bending facilitates the movement of larger ions toward the convex sign of the bent film. Such a

Citation: Rajapaksha, C.P.H.; Gunathilaka, M.D.T.; Narute, S.; Albehaijan, H.A.; Piedrahita, C.; Paudel, P.; Feng, C.; Lüssem, B.; Kyu, T.; Jákli, A. Flexo-ionic Effect of Ionic Liquid Crystal Elastomers. *Molecules* **2021**, 26, x. https://doi.org/10.3390/xxxxx

Received: date
Accepted: date
Published: date

Publisher's Note: MDPI stays neutral with regard to jurisdictional claims in published maps and institutional affiliations.



Copyright: © 2021 by the authors. Submitted for possible open access publication under the terms and conditions of the Creative Commons Attribution (CC BY) license (http://creativecommons.org/licenses/by/4.0/).

mechanism provides low voltage operation for actuators, and large current response for sensing, thus making them attractive for various applications.

Recently, a new class of strain gradient induced electric current was demonstrated in ionic polymer membranes 9 . In appearance, this effect is similar to the flexoelectric effect, except that, instead of the displacement of bound charges, here positive and negative ions move in opposite directions due to mechanical bending $^{6-9,26}$. To express this difference, we shall call this effect as flexo-ionic effect. Indeed, the flexo-ionic coefficients of these materials are much larger (29–323 $\mu C/m$) than those of the flexoelectric coefficients of insulating polymers. The flexo-ionic effect in its nature is the converse of the electro-actuation of ionic polymers and elastomers (iEAPs) containing different sizes of cations and anions $^{3,23,27-36}$.

Most recently, our group has demonstrated electro-actuation of a new class of materials, ionic liquid crystal elastomers ¹. We showed that iLCEs can be actuated by low frequency AC or DC voltages of less than 1 V with bending strains comparable to the well-developed iEAPs. It was also shown that the fastest and strongest electro actuation is observed for films where the director is uniformly parallel to the substrates (planar alignment). This implies the possibility of pre-programed actuation pattern at the stage of cross-linking process, and dual (thermal and electric) actuations in hybrid samples.

Here, we report the study of the converse effect, the flexo-ionic effects of iLCEs. Similar to electro-actuation, we find a strong alignment dependence of the flexo-ionic effect that is comparable to those found in ionic polymer membranes.

2. Results and Discussion

POM images of 200 μm thick iLCE samples prepared as will be described in the Materials and Method section and cross-linked in the isotropic phase; in the nematic phase between planar and homeotropic alignment substrates; and in hybrid alignment (between planar and homeotropic substrates) are shown in the 1st to 4th columns from left to the right, respectively in Figure 1. For the sake of brevity, these materials will be referred as isotropic, planar, homeotropic and hybrid samples, respectively. The top row (a-d) shows the top view of iLCE samples between cross polarizers in transmission. As depicted in Figure 1a, the isotropic sample appeared to be completely dark, confirming the optical isotropy of the film. Bright droplets in the dark (isotropic) background in Figure 1b-d indicate spinodal decomposition of the isotropic ionic liquid-rich and the birefringent (bright) nematic LCE-rich phase ³⁷. The decomposition was induced by the isotropic-nematic transition and was found to strongly depend on the time the sample stayed in the nematic phase before the completion of crosslinking reaction. After crosslinking, the phase separation is halted, and the size of the birefringent and isotropic domains did not change. For this reason, the crosslinking reaction was carried out at ~50°C, only a few degrees below the I-N transition.

The middle row (e-h) of Figure 1, displays the top view of iLCE samples in reflection. The surface morphology of the isotropic film (e) is smooth, while the surface morphology of planar (f), homeotropic (g), and hybrid (h) show inhomogeneous structures due to the phase separation between ionic liquid and nematic liquid crystal rich phases.

Even though, due to the phase separation, there is no significant differences in the textures in top views between the samples cross-linked in the nematic phase, there is a significant difference in the side views as seen in the bottom row of Figure 1. Similar to the transmission images, the isotropic (i) sample is uniform, while the planar (*j*), homeotropic (*k*) and hybrid (*l*) samples are inhomogeneous. Notably, while the top views of the planar and the hybrid (with planar side on the top) samples are darker (less reflective) than of the isotropic and the homeotropic cells, the side views of the planar and isotropic samples are brighter (more reflective) than the homeotropic cell. Additionally, the hybrid cell shows a sharp contrast between bright texture closer to the planar surface and darker near the homeotropic substrate. Since in the side view, the planar director points toward the picture, we conclude that the ionic channels that reflect light have larger cross sections

in the plane normal to the LCE director. These show that, although the surface alignments are somewhat disturbed by the phase separation, the bulk alignments are clearly influenced by the surface alignments.

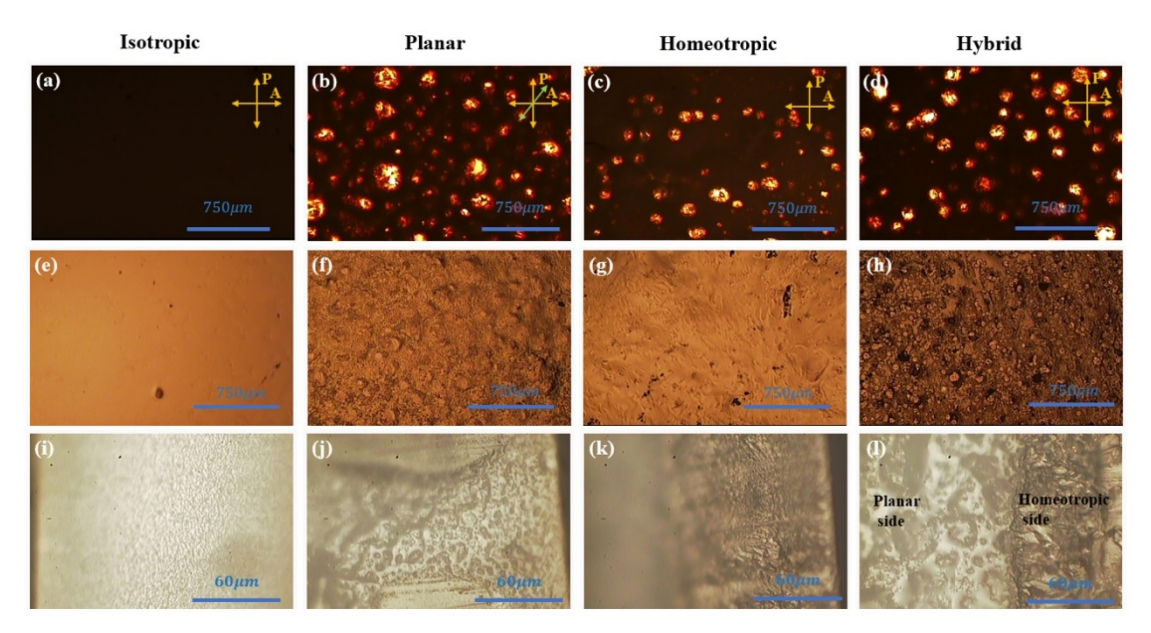


Figure 1. POM images of 200-μm thick iLCE samples cross-linked in the isotropic phase (first column), in the nematic phase between planar alignment substrates (second column), between homeotropic alignment substrates (third column), and in hybrid alignment between planar (top) and homeotropic (bottom) substrates (fourth column). First row: top view of iLCE samples between cross polarizers in transmission. Second row: top view of iLCEs in reflection mode. Third row: cross section of iLCEs in reflection (the substrates are on the left and right and the director in planar alignment points normal to the picture plane).

As expected, DSC measurements revealed that the glass transition temperatures (T_g) for all samples are the same ($T_g \sim 22^{\circ}$ C). This indicates that the plasticization of iLCE is independent of the director alignment and depends only on the composition of the polymer matrix.

The tensile stress-strain curves of the different iLCE strips are not linear even at small strains, which indicates strain-induced director realignment and/or ionic channel reconfigurations. The slopes give Young's moduli values in the range of 1-3MPa, that are several times smaller than typical values of the pure LCEs. This implies that the ion channels have weakened the elastomeric networks. The maximum applicable strain before rupturing depends on the alignment; the isotropic film can be strained up to ~ 50 %, while the hybrid, homeotropic and planar films rupture at ~ 25 %, ~ 12 %, and ~ 10 % strain, respectively. The threshold for the rupture is likely related to the structure of defects and phase separation, which are largely absent in the isotropic film and differently aligned in the planar and homeotropic cells.

The DC ionic conductivities σ of the samples are calculated using the equation $\sigma = L/RA$, where L is the thickness of the film, R is the resistance, and A is the active area of the film. The ionic conductivities are found to be 3.3 mS/m, 2.5 mS/m, 0.18 mS/m, and 0.03 mS/m for the planar, isotropic, homeotropic, and hybrid alignment respectively. The high ionic conductivities of planar and isotropic samples and low ionic conductivities of the homeotropic and hybrid samples are consistent with the reflection images that indicated that the ionic channels that reflect light, have larger cross sections in the plane normal to the LCE director, which is along the film thickness in the planar cells. Additionally, the boundary interface seen in the middle of the cross-section of the hybrid film appears to block the ion transportation through the film, resulting in the lowest ionic conductivity.

The measured time dependences of the electric currents, in response to sinusoidal and square-wave (intermittent) cantilever bending, are depicted in Figure 2a and b,

respectively. As shown in Figure 2a, the current response follows the sine wave with the same $1\,Hz$ frequency. Figure 2b exhibits spikes during the intermittent bending following the direction of the intermittent bending with T = 100 s periodicity.

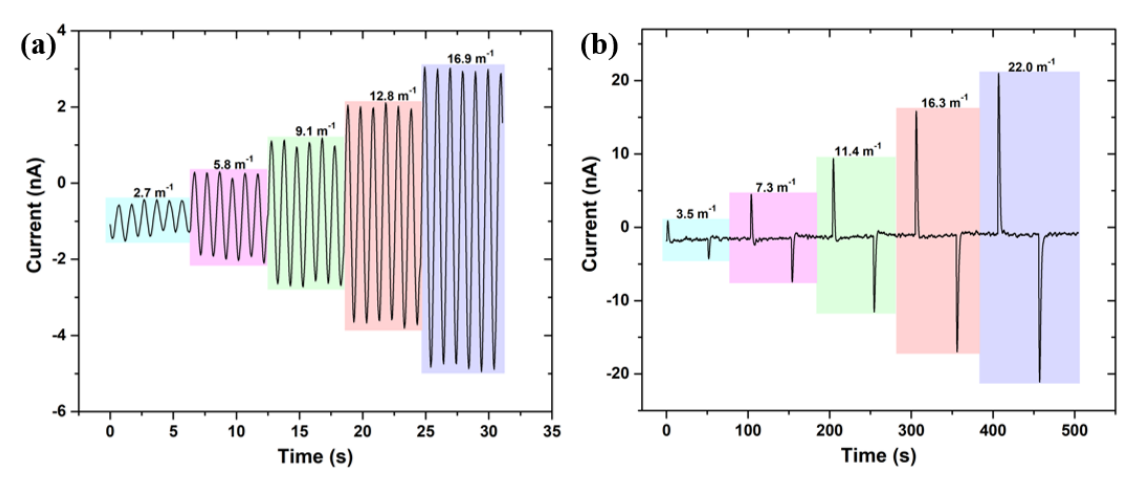


Figure 2. Flexo-ionic effect due to sinusoidal and intermittent cantilever bending a) Current response due to sine wave (1 Hz) bending with different curvatures b) Current response due to a square wave (10 mHz) bending with different curvatures.

The bending-induced ionic current is due to the ion motion driven by the pressure gradient, which pushes the larger cations from the compressed (low volume) higher pressure side toward the expanded (high volume) low pressure side. Simultaneously, the smaller anions move in opposite directions. This leads to a charge separation that can be characterized by an effective dipole moment μ with a dimension of charge times distance, which is the net charge at the two substrates multiplied by the film thickness, $\mu = Q \cdot d$. The flexo-ionic polarization P_{f-i} , i.e., the dipole density can be expressed as $P_{f-i} = \frac{\mu}{V} = Q/A$, where A is the electrode area. The net charge Q can be obtained by the time integral of the measured ionic current I as $Q = \int_0^T I \, dt$, where T, the period of the bending is the inverse of the bending frequency, T = 1/f. From these, we get the flexo-ionic polarization from the measured ionic current generated under the bending frequency f, as

$$P_{f-i} = I/2\pi f A \tag{1}$$

The flexo-ionic polarization calculated by Eq. (1) is plotted as the function of the curvature for sinusoidal and square-wave bending are shown in Figure 3a and b, respectively.

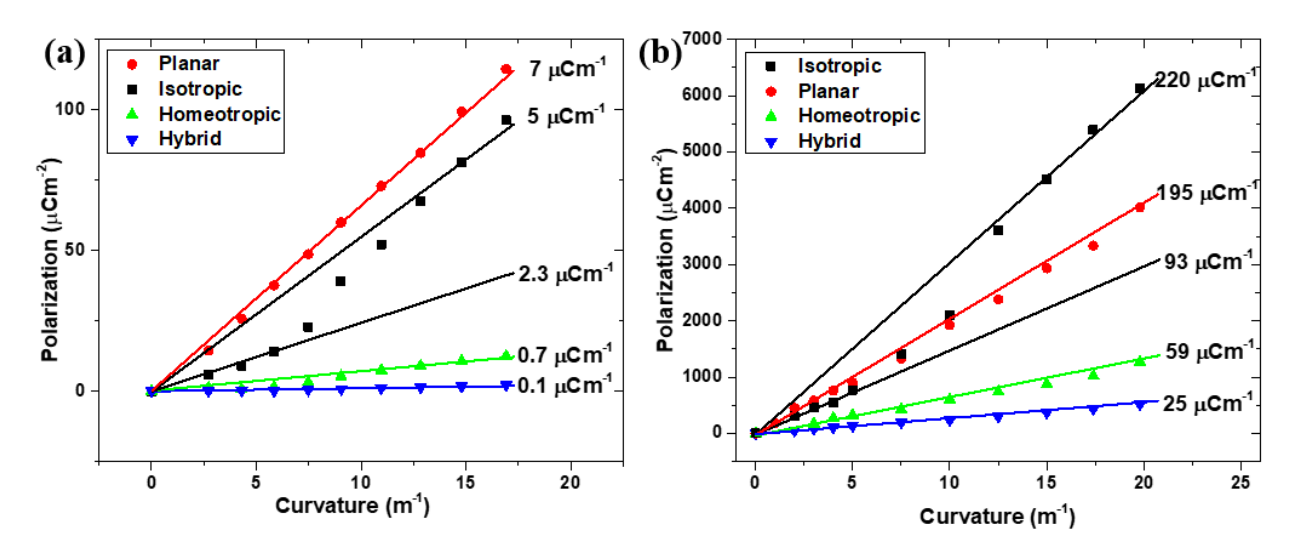
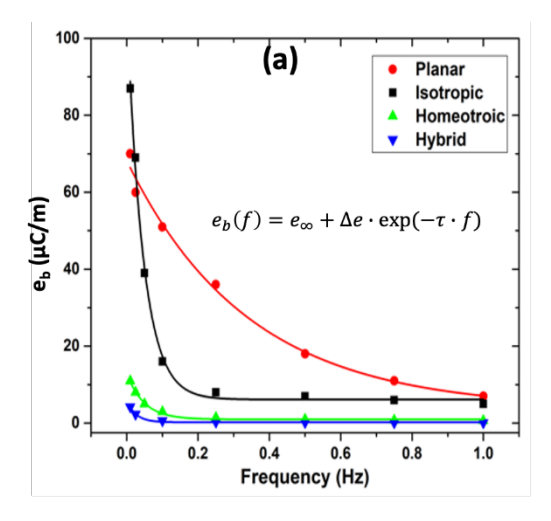


Figure 3. Flexo-ionic polarization versus bending curvature of differently aligned iLCEs samples. (a) 1 Hz sine wave bending (b) 10 mHz square wave mechanical deformation.

We see that the flexo-ionic polarization is basically proportional to the curvature for all samples that were crosslinked in the nematic phase, whereas the isotropic sample shows two linear regimes with a smaller slope at curvatures $\kappa < 6~m^{-1}$ and a larger slope at $\kappa > 12~m^{-1}$. The slopes determine the flexo-ionic coupling constant, $e_b = P_{f-i}/\kappa$. In comparing Figure 3a and b, one can see that for the 1 Hz sine wave bending e_b is largest $(e_b = 7\mu C/m)$ for the planar sample and smallest $(e_b = 0.1~\mu C/m)$ for the hybrid sample. On the other hand, for the 10 mHz square wave bending, the flexo-ionic coefficients are more than an order of magnitude larger. Similar to the 1 Hz sinusoidal bending, for $\kappa < 6~m^{-1}$ curvatures the largest coefficient is obtained in planar samples $(e_b = 195\mu C/m)$ followed by the isotropic $(e_b = 93\mu C/m)$, homeotropic $((e_b = 59\mu C/m))$ and hybrid $(e_b = 25\mu C/m)$ samples. At $\kappa > 12~m^{-1}$ curvatures however the isotropic sample overcomes by the planar $e_b = 220\mu C/m$ bending flexo-ionic coefficient.

To find out if the large differences in the flexo-ionic coefficients were due to the difference in the time dependence of the bending (sine or square wave) or simply due to the difference in frequencies, we measured the frequency dependence of the flexo-ionic coefficients, e_b in sine wave excitation only. The results are plotted in Figure 4a. One can see that at very low frequencies (below 0.02 Hz) the isotropic sample has the largest response, but that decreases very quickly and above 0.03 Hz the planar cell overcomes all other alignments. The extrapolated e_b at $10 \, mHz$ becomes comparable with the results obtained in 10 mHz rectangular voltages, indicating that this is the main factor responsible for the differences seen in Figure 3a and b are due to the frequency and not the waveform. Best exponential fits to the frequency dependences of the time constant τ give 2.9 s for planar, 22.1 s for the isotropic, 20.7 s for the homeotropic and 38.7 s for the hybrid films. These values, within the experimental errors, are corroborated with the alignment dependences of the electric conductivity and are in agreement with those observed for the response times of the same materials in electro-actuation 1. The non-zero e_{∞} values for the planar and isotropic samples indicate that a small portion of the sample reacts even faster (above 1 Hz).

To obtain an insight to the nature of the reproducibility, we have carried out the measurements both in increasing and decreasing curvatures for all materials. Within the error, no hysteresis has been observed for any of the samples, including the isotropic sample, where the slope varies with the curvature. This latter one is shown in Figure 4b. The change of the slope at increasing curvature indicates a strain-gradient induced alignment of the mesogenic side chains from an isotropic distribution to an aligned structure. As the slope in the high bend region is closest to that of the planar sample, we conjecture that the bending induced alignment is planar. The fact that in this range the isotropic strip shows an even larger flexo-ionic effect than the planar sample, is probably due to the weaker phase separation and the lack of defects. The lack of hysteresis indicates that this realignment is completely reversible, i.e., the isotropic distribution of the director structure resumes reversibly.



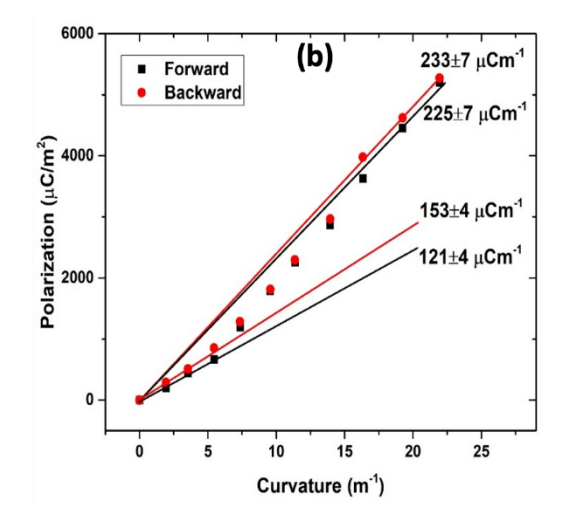


Figure 4. (a) Frequency dependence of the flexo-ionic coefficient of differently aligned iLCEs. Symbols are the experimental data points, and the solid lines are fitted curve to a single exponential function with the equation shown in the figure. (b) Flexo-ionic polarization versus increasing and decreasing curvature for the isotropic sample. The error values indicated in the figure are calculated by the standard deviation. Black solid squares denote the polarization measured during the curvature increment and solid red circles denote the polarization measured during the curvature decrement.

3. Materials and Methods

3.1. Materials

Monofunctional acrylate monomer M1 (4-(6-Acryloxy-hex-1-yl-oxy) phenyl-4-(hexyloxy) benzoate) and bifunctional crosslinker M2 (1,4-Bis- [4-(6- acryloyloxyhexyloxy) benzoyloxy]-2-methylbenzene) were purchased from Synthon chemicals. IL (1-Hexyl-3-methylimidazolium hexafluorophosphate (HMIM-PF6)) and photoinitiator (2,2- Dimethoxy-2-phenylacetophenone (Irgacure® 651)) were acquired from Sigma-Aldrich. The molecular structures of these materials are illustrated in Figure 5a. For planar alignment polyimide PI-2555, and for homeotropic alignment PI-5661 alignment coatings were used as received from HD MicroSystems. For electrode materials, PEDOT:PSS (Clevios™ PH1000) was mixed with 5% ethylene glycol (EG) and 0.25% dodecyl benzene sulfonic acid (DBSA) to enhance the conductivity ³⁸.

3.2. Sample Preparations

M1, M2, and the photo initiator were mixed in 87:12:1 weight ratio to form the LCE precursors. Subsequently, an ionic liquid (HMIM-PF6) was added to the LCE precursor solution and mechanically stirred for 15 minutes after heating to 80°C to achieve complete mixing. A re-determined weight percentage (25%) of ionic liquid was used as per our previous experience on this system for electric actuation ¹.

The substrate preparation and iLCE film fabrication are illustrated in Figure 5b and c. To prepare the planar aligned and homeotropically aligned glass substrates (see Figure 5b), 25 mm by 25 mm glass pieces were sonicated for 20 minutes at 60°C and washed with distilled water and isopropyl alcohol (IPA) followed by drying at 90°C for 20 minutes. Afterward, a 10 nm thick layer of polyimide PI-2555, and PI-5661 was spin-coated on the glass substrates for planar and homeotropic alignments, respectively. After soft baking at 60°C, the homeotropic alignment layer were hard-baked at 160 °C for 1 hour and the planar alignment polyimide film was hard-baked at 200 °C for 1 hour and was rubbed unidirectionally with velvet cloth.

Four types of iLCE samples were prepared. One sample was cross-linked in the isotropic phase (called "Isotropic" sample) between two cleaned glass substrates with no alignment layer. Three were cross-linked in the nematic phase between planar alignment substrates ("Planar" sample), between homeotropic alignment substrates ("Homeotropic" sample), and in hybrid alignment between planar and homeotropic substrates ("Hybrid"

sample). Figure 5c shows the steps to prepare 200 μ m thick cells using capillary fill, UV irradiation for cross-linking, then peeling off the iLCE, coating both sides by PEDOT: PSS to achieve the freestanding films with electrodes.

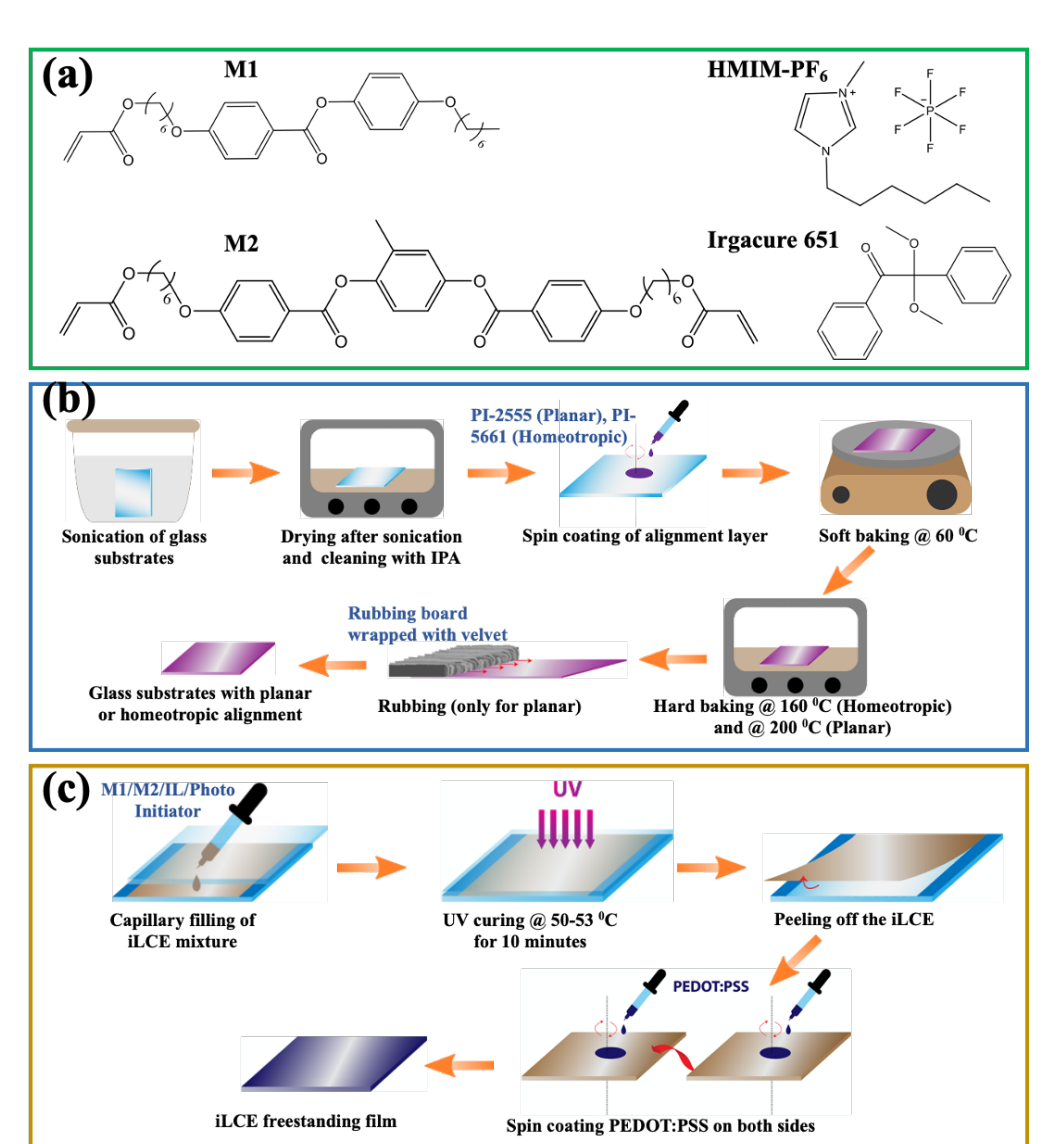


Figure 5. Molecular structures of the components of the iLCE materials and the illustration of sample preparation. (a) Molecular structures of the components of the studied iLCE: M1 and M2 are mesogenic units, HMIM-PF₆ is the ionic liquid and Irgacure 651 is the photoinitiator. (b) Schematic view of preparation of the planarly and homeotropically aligned glass substrates. (c) Schematic view of fabrication of differently aligned (planar, homeotropic, hybrid, isotropic) iLCE films with PEDOT:PSS electrodes.

The iLCE mixtures were filled to 200 μ m cells at 80°C (in the isotropic phase) by capillary action. Planar, homeotropic and hybrid samples were photopolymerized under 365 nm UV light (Black-Ray, Model B-100AP/R) in the nematic phase (50-55°C) for 10 minutes, while the isotropic sample was crosslinked in the isotropic phase (80°C) under the same condition. Afterward, the iLCE films were peeled off from the glass substrates, and about 100 nm thick PEDOT: PSS electrodes were spin-coated on both sides. Finally, the iLCE freestanding films with electrodes were cut into 2 mm by 15 mm pieces for material characterization and for the flexo-ionic measurements.

39.

258

259

260

261

262

263

264

265

266

267

268

269

270

271

272

273

274

275

276

277

278

279

280

281

282

283

284

The top views and the cross sections of iLCE samples were captured using a Polarized Optical Microscope (POM) from Olympus (model: BX60) in transmission and reflection modes.

The glass transition temperatures (Tg) of iLCE films with different director alignments were determined by Differential Scanning Calorimetry (DSC) using Model Q200 from Thermal Analysis Instruments Inc., TA. Samples weighing 5-10 mg were hermetically sealed in aluminum pans by using a clamping machine. An empty aluminum pan was used for reference. Thermal scans were performed under nitrogen gas flow from -75 °C to 50 °C with a scan-rate of 10 °C/min.

The tensile properties were determined using a dynamic mechanical analyzer (DMA Q800, TA Instruments). The instrument was operated under tension mode with an initial strain rate of 1% at room temperature.

To investigate the ionic conductivities of the four types of iLCE samples, 50 mV DC and 1 mHz square wave voltages were applied across the iLCE films, and the electric current was measured.

The flexo-ionic effects of iLCE films were studied using a home-made setup as illustrated in Figure 6a. Sinusoidal and square-wave oscillatory deformation were generated using a mechanical vibrator (SF-9324, PASCO) driven by a function generator (Agilent, 33120A). The ionic currents generated by the bending deformations were measured using an electrometer (6517B, Keithley) connected to a computer interface via GPIB (General Purpose Interface Bus) port by using a home-made LabView script. To determine the tip displacement y of the film, the images of bending were captured by a high-speed camera (Pixelink, 742000782) mounted to microscope (Wild, M5-71977). A home-made Matlab (2019b) image processing script was used to analyze images. The bending curvature κ of an iLCE film was calculated from the tip displacement y using the equation

$$\kappa = \frac{1}{u} \frac{\text{Slu} - 1/2 \text{ Su}^2}{\sqrt{1 + (\text{Slu} - 1/2 \text{ Su}^2)^2}}$$
 (2)

where 2*l* is the distance between clamps *u* is the active sample length and $S = \frac{3y}{213}$

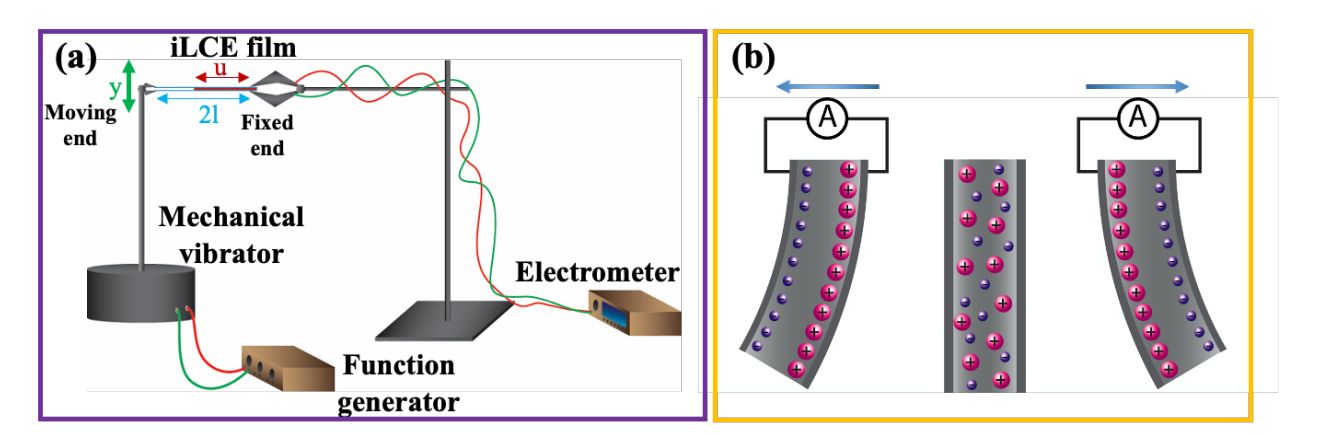


Figure 6. The schematic of the experimental setup, and the illustration of the physical mechanism of the flexo-ionic effect. (a) The schematic of the experimental setup to study flexo-ionic effect. (b) Illustration of the principle of the flexo-ionic effect.

The principle of the physical mechanism leading to the bending-induced ionic current is illustrated in Figure 6b.

4. Conclusions

We presented the first flexo-ionic effects of ionic Liquid Crystal Elastomer samples in 4 different director configurations, isotropic, planar, homeotropic and hybrid. We

285

286 287 288

289 290

291 292

295

296

297

298

299

300

301

302

303

304

305

306

307

308

309

310

311

found that the measured flexo-ionic coupling constants strongly depend on the director structures and on the frequency of the mechanical bending. Morphology measurements carried out by POM and electric conductivity measurements show that the liquid crystal director structure and the phase of the liquid crystal where the cross-linking happens critically determines the structure and distribution of the ionic liquid channels. It appears that the cells cross-linked in the isotropic phase and that are crosslinked in the nematic phase between planar alignment substrates give the largest response with flexo-ionic coefficients ~200μC/m. Such coefficients are comparable to the well-developed iEAPs 6.9. It is interesting to discern that the flexo-ionic coefficients of iLCEs outperform the flexoelectric (polarization mechanism is different) coefficients of ceramics (PZT12 and Ba0.67Sr0.33TiO3 40), crystalline polymers (PVDF) 41, and bent-core liquid crystals 18,19. This finding shows that at very low frequencies, the bending induced charge separation of differently sized cations and anions of ionic liquids dispersed in polymers and liquid crystal elastomers are much more effective to lead to polarization than separation of bound charges in insulating media. Our results, therefore, imply the possible use of iLCEs in sensors and energy harvesting devices where the mechanical excitations are slow (below 0.1 Hz). Further, ILCEs without spinodal decomposition is under investigation for the applications of soft actuators, sensors, and energy harvesting devices.

Table 1. Comparison of flexo-ionic coefficient and limit of the driving frequencies of iLCEs with ionic electroactive polymers, bent-core liquid crystals and insulating polymers and ceramics.

Materials	Flexoelectric/ Ionic Coefficient	Driving Frequencies
iLCEs (This study)	25 - 220 μC/m	0.01 – 1 Hz
PEM (TS-PEGDA/IL)	$84 - 154 \ \mu C/m^6$	0.01 - 10 Hz
PEM (PEGDA/IL)	$53 - 125 \ \mu C/m^6$	0.01 – 1 Hz
PEM (PEGDA/SCN/LiTFSI)	29 - 323 μC/m ⁴²	0.01 Hz
bent-core liquid crystal	60 n <i>C/m</i> 18	1-10 Hz
Bent-core liquid crystal elastomer	30 nC/m 19	0.2 – 12 Hz
PVDF	2 - 13 nC/m ⁴¹	6 Hz
Pb [Zr _x Ti _{1-x}] O ₃ (PZT)	$1.4~\mu C/m^{-12}$	1 Hz
Ba0.67Sr0.33TiO3	100 μC/m ⁴⁰	2 Hz

Acknowledgments: This work was supported by the Physics Department of Kent State University and the National Science Foundation (DMR-1904167 and ECCS 1750011).

References

(1) Feng, C.; Rajapaksha, C. P. H.; Cedillo, J. M.; Piedrahita, C.; Cao, J.; Kaphle, V.; Lussem, B.; Kyu, T.; Jákli, A. I. Electro-Responsive Ionic Liquid Crystal Elastomers. *Macromol. Rapid Commun.* **2019**, 1900299. https://doi.org/DOI: 10.1002/marc.201900299.

(2) Rajapaksha, C. P. H.; Feng, C.; Piedrahita, C.; Cao, J.; Kaphle, V.; Lüssem, B.; Kyu, T.; Jákli, A. Poly(Ethylene Glycol)
Diacrylate Based Electro-Active Ionic Elastomer. *Macromol. Rapid Commun.* **2020**, 41 (6), 1900636.
https://doi.org/10.1002/marc.201900636.

(3) Kim, O.; Kim, S. J.; Park, M. J. Low-Voltage-Driven Soft Actuators. Chem. Commun. 2018, 54, 4895–4904.

312 313

314 315

316

317 318

319

320 321

325

326

329

330

331

332

333

334

338

339

340

341

342

343

344

345

346

347

348

349

352

353

358

359

363

364

- https://doi.org/10.1039/C8CC01670D.
- (4) Feng, C.; Hemantha Rajapaksha, C. P.; Jákli, A. Ionic Elastomers for Electric Actuators and Sensors. *Engineering* **2021**. https://doi.org/10.1016/j.eng.2021.02.014.
- (5) Wu, J. M.; Chen, C. Y.; Zhang, Y.; Chen, K. H.; Yang, Y.; Hu, Y.; He, H.; Wang, Z. L. Ultrahigh Sensitive Piezotronic Strain 327 Sensors Based on a ZnSnO 3 Nanowire/Microwire. *ACS Nano* 2012, 6 (5), 4369–4374. https://doi.org/10.1021/nn3010558.
- (6) Piedrahita, C. R.; Yue, P.; Cao, J.; Lee, H.; Rajapaksha, C. P.; Feng, C.; Jákli, A.; Kyu, T. Flexoelectricity in Flexoionic Polymer Electrolyte Membranes: Effect of Thiosiloxane Modification on Poly(Ethylene Glycol) Diacrylate and Ionic Liquid Electrolyte Composites. *ACS Appl. Mater. Interfaces* **2020**, *12* (14), 16978–16986. https://doi.org/10.1021/acsami.0c02328.
- (7) Albehaijan, H. A.; Piedrahita, C. R.; Cao, J.; Soliman, M.; Mitra, S.; Kyu, T. Mechanoelectrical Transduction of Polymer Electrolyte Membranes: Effect of Branched Networks. *ACS Appl. Mater. Interfaces* **2020**, 12 (6), 7518–7528. https://doi.org/10.1021/acsami.9b15599.
- (8)A. Albehaijan, H.; Cao, J.; R. Piedrahita, C.; Jákli, A.; Kyu, T. Role of Cationic Size and Valency in Mechanoelectrical 335 Transduction of **Ion-Containing** Polymers. **ACS** Sustain. Chem. & Eng. 2021, (0).336 https://doi.org/10.1021/acssuschemeng.0c08252. 337
- (9) Cao, J.; Piedrahita, C.; Kyu, T. Mechanoelectrical Conversion in Highly Ionic Conductive Solid-State Polymer Electrolyte Membranes. *Macromol. Mater. Eng.* **2019**, 304 (5), 1800777. https://doi.org/10.1002/mame.201800777.
- (10) Ikeda, T. Piezoelectricity and Pyroelectricity. In *Fundamentals of Piezoelectricity*; Oxford University Press: New York, 1990; pp 1–30.
- (11) Mayer, R. M. Piezoelectric Effects in Liquid Crystals. Phys. Rev. Lett. 1969, 22 (July), 25–29.
- (12) Ma, W.; Cross, L. E. Flexoelectric Effect in Ceramic Lead Zirconate Titanate. *Appl. Phys. Lett.* **2005**, *86* (7), 1–3. https://doi.org/10.1063/1.1868078.
- (13) Ma, W. Flexoelectricity: Strain Gradient Effects in Ferroelectrics. *Phys. Scr.* **2007**, No. T129, 180–185.
- (14) Chu, B.; Salem, D. R. Flexoelectricity in Several Thermoplastic and Thermosetting Polymers. *Appl. Phys. Lett.* **2012**, *101* (10). https://doi.org/10.1063/1.4750064.
- (15) Marvan, M.; Havránek, A. Flexoelectric Effect in Elastomers. In *Relationships of Polymeric Structure and Properties*; Steinkopff: Darmstadt, 2007; Vol. 36, pp 33–36. https://doi.org/10.1007/BFb0114342.
- (16) SCHMIDT, D. .; SCHADT, M. .; HELFRICH, W. . Liquid-Crystalline Curvature Electricity: The Bending Mode of MBBA. Z. 350 Naturforsch 1972, 26A, 277–280.
- (17) Buka, Á.; Éber, N. *Flexoelectricity in Liquid Crystals*, 1st ed.; Buka, A., Eber, N., Eds.; IMPERIAL COLLEGE PRESS: London, 2013. https://doi.org/10.1142/p812.
- (18) Harden, J.; Mbanga, B.; Iber, N.; Fodor-Csorba, K.; Sprunt, S.; Gleeson, J. T.; Jákli, A. Giant Flexoelectricity of Bent-Core 354

 Nematic Liquid Crystals. *Phys. Rev. Lett.* **2006**, *97* (15), 13–16. https://doi.org/10.1103/PhysRevLett.97.157802. 355
- (19) Harden, J.; Chambers, M.; Verduzco, R.; Luchette, P.; Gleeson, J. T.; Sprunt, S.; Jákli, A. Giant Flexoelectricity in Bent-Core
 Nematic Liquid Crystal Elastomers. *Appl. Phys. Lett.* **2010**, *96* (10). https://doi.org/10.1063/1.3358391.
- (20) Kim, O.; Kim, H.; Choi, U. H.; Park, M. J. One-Volt-Driven Superfast Polymer Actuators Based on Single-Ion Conductors. *Nat. Commun.* **2016**, *7*, 13576–13584. https://doi.org/10.1038/ncomms13576.
- (21) Kim, O.; Kim, S. Y.; Park, B.; Hwang, W.; Park, M. J. Factors Affecting Electromechanical Properties of Ionic Polymer 360 Actuators Based on Ionic Liquid-Containing Sulfonated Block Copolymers. *Macromolecules* 2014, 47 (13), 4357–4368. 361 https://doi.org/10.1021/ma500869h.
- (22) Kim, O.; Shin, T. J.; Park, M. J. Fast Low-Voltage Electroactive Actuators Using Nanostructured Polymer Electrolytes. *Nat. Commun.* **2013**, *4*, 3208. https://doi.org/10.1038/ncomms3208.
- (23) Lee, J.; Aida, T. "Bucky Gels" for Tailoring Electroactive Materials and Devices: The Composites of Carbon Materials with

- Ionic Liquids. Chem. Commun. 2011, 47 (24), 6757–6762. https://doi.org/10.1039/c1cc00043h.
- (24) Bahramzadeh, Y.; Shahinpoor, M. A Review of Ionic Polymeric Soft Actuators and Sensors. *Soft Robot.* **2013**. https://doi.org/10.1089/soro.2013.0006.
- (25) Wei, D.; Ivaska, A. Applications of Ionic Liquids in Electrochemical Sensors. *Anal. Chim. Acta* **2008**, 607 (2), 126–135. 369 https://doi.org/10.1016/j.aca.2007.12.011.
- (26) Cao, J.; Rendon Piedrahita, C.; Zhao, Z.; Vogt, B. D.; Kyu, T. Tuning Flexoelectric Effect in Polymer Electrolyte Membranes via Cation Selection for Potential Energy Harvesting Applications. *ACS Appl. Energy Mater.* **2020**, *3*, 328–335. https://doi.org/10.1021/acsaem.9b01572.
- (27) Margaretta, E.; Fahs, G. B.; Inglefield, D. L.; Jangu, C.; Wang, D.; Heflin, J. R.; Moore, R. B.; Long, T. E. Imidazolium-Containing ABA Triblock Copolymers as Electroactive Devices. *ACS Appl. Mater. Interfaces* **2016**, *8* (2), 1280–1288. https://doi.org/10.1021/acsami.5b09965.
- (28) Gao, R.; Wang, D.; Heflin, J. R.; Long, T. E. Imidazolium Sulfonate-Containing Pentablock Copolymer-Ionic Liquid Membranes for Electroactive Actuators. *J. Mater. Chem.* **2012**, 22 (27), 13473–13476. https://doi.org/10.1039/c2jm16117f.
- (29) Bar-Cohen, Y. *Electroactive Polymer (EAP) Actuators as Artificial Muscles: Reality, Potential, and Challenges;* SPIE press Bellingham, WA, 2004; Vol. 136.
- (30) Takeuchi, I.; Asaka, K.; Kiyohara, K.; Sugino, T.; Terasawa, N.; Mukai, K.; Fukushima, T.; Aida, T. Electromechanical Behavior of Fully Plastic Actuators Based on Bucky Gel Containing Various Internal Ionic Liquids. *Electrochim. Acta* 2009, 54 (6), 1762–1768. https://doi.org/10.1016/j.electacta.2008.10.007.
- (31) Imaizumi, S.; Kato, Y.; Kokubo, H.; Watanabe, M. Driving Mechanisms of Ionic Polymer Actuators Having Electric Double Layer Capacitor Structures. *J. Phys. Chem. B* **2012**, *116* (16), 5080–5089. https://doi.org/10.1021/jp301501c.
- (32) Fukushima, T.; Asaka, K.; Kosaka, A.; Aida, T. Fully Plastic Actuator through Layer-by-Layer Casting with Ionic-Liquid-Based Bucky Gel. *Angew. Chemie Int. Ed.* **2005**, 44 (16), 2410–2413. https://doi.org/10.1002/anie.200462318.
- (33) Asaka, K.; Mukai, K.; Sugino, T.; Kiyohara, K.; Takeuchi, I.; Terasawa, N.; Aida, T.; Futaba, D. N.; Hata, K.; Fukushima, T. Highly Conductive Sheets from Millimeter-Long Single-Walled Carbon Nanotubes and Ionic Liquids: Application to Fast-Moving, Low-Voltage Electromechanical Actuators Cperable in Airs. *Adv. Mater.* **2009**, *21* (16), 1582–1585. https://doi.org/10.1002/adma.200802817.
- [34] Jangu, C.; Wang, J. H. H.; Wang, D.; Fahs, G.; Heflin, J. R.; Moore, R. B.; Colby, R. H.; Long, T. E. Imidazole-Containing Triblock Copolymers with a Synergy of Ether and Imidazolium Sites. *J. Mater. Chem. C* 2015, 3 (16), 3891–3901. https://doi.org/10.1039/c5tc00169b.
- (35) Lee, J. W.; Yu, S.; Hong, S. M.; Koo, C. M. High-Strain Air-Working Soft Transducers Produced from Nanostructured Block Copolymer Ionomer/Silicate/Ionic Liquid Nanocomposite Membranes. *J. Mater. Chem. C* **2013**, *1* (24), 3784–3793. https://doi.org/10.1039/c3tc30414k.
- (36) Green, M. D.; Wang, D.; Hemp, S. T.; Choi, J. H.; Winey, K. I.; Heflin, J. R.; Long, T. E. Synthesis of Imidazolium ABA Triblock Copolymers for Electromechanical Transducers. *Polymer (Guildf)*. **2012**, 53 (17), 3677–3686. https://doi.org/10.1016/j.polymer.2012.06.023.
- (37) Binder, K. Collective Diffusion, Nucleation, and Spinodal Decomposition in Polymer Mixtures. *J. Chem. Phys.* **1983**. https://doi.org/10.1063/1.445747.
- (38) Kaphle, V.; Liu, S.; Al-Shadeedi, A.; Keum, C.-M.; Lüssem, B. Contact Resistance Effects in Highly Doped Organic 403 Electrochemical Transistors. *Adv. Mater.* **2016**, *28* (39), 8766–8770. https://doi.org/10.1002/adma.201602125.
- (39) Cao, J. Bioelectricity Inspired Polymer Electrolyte Membranes for Sensing and Engergy Harvesting Applications, 2018.
- (40) Kwon, S. R.; Huang, W.; Shu, L.; Yuan, F. G.; Maria, J. P.; Jiang, X. Flexoelectricity in Barium Strontium Titanate Thin Film. 406

 Appl. Phys. Lett. 2014, 105 (14). https://doi.org/10.1063/1.4898139.

(41)	Zhou, Y.; Liu, J.; Hu, X.; Chu, B.; Chen, S.; Salem, D. Flexoelectric Effect in PVDF-Based Polymers. IEEE Trans. Dielectr. Electr.
	Insul. 2017, 24 (2), 727–731. https://doi.org/10.1109/TDEI.2017.006273.
(42)	Cao, J.; Piedrahita, C.; Kyu, T. Mechanoelectrical Conversion in Highly Ionic Conductive Solid-State Polymer Electrolyte

Membranes. Macromol. Mater. Eng. 2019, 1800777, 1800777. https://doi.org/10.1002/mame.201800777.